

Supporting Information for

**Metal oxide plating for maximizing the performance in
ruthenium(IV) oxide-catalyzed electrochemical oxygen
evolution reaction**

Shin-ichi Naya,^a Mio Nagamitsu,^b Hisashi Sugime,^{b,c} Tetsuro Soejima,^{b,c} Hiroaki Tada^{d*}

¹ Environmental Research Laboratory, Kindai University, 3-4-1, Kowakae, Higashi-Osaka, Osaka 577-8502, Japan.

² Graduate School of Science and Engineering, Kindai University, 3-4-1, Kowakae, Higashi-Osaka, Osaka 577-8502, Japan.

³ Department of Applied Chemistry, Faculty of Science and Engineering, Kindai University, 3-4-1, Kowakae, Higashi-Osaka, Osaka 577-8502, Japan.

⁴ Institutes of Innovation for Future Society, Nagoya University, Furo-cho, Chikusa-ku, Nagoya Aichi 464-8603, Japan.

* To whom correspondence should be addressed to Professor Hiroaki Tada

E-mail: htada0409@gmail.com

Table of Contents

Materials and experimental methods.	S3-S4
Table S1. Comparison of the mass-specific activity of ST-RuO ₂ //TiO ₂ NWA and the RuO ₂ electrodes with the references.	S5-S6
Table S2. Peak area ratio of O1s-XP signals for ST-RuO ₂ (<i>x</i>)//TiO ₂ NWA and Im-RuO ₂ //TiO ₂ electrodes.	S7
Table S3. EIS parameters for ST-RuO ₂ (<i>x</i>)//TiO ₂ NWA and Im-RuO ₂ //TiO ₂ electrodes.	S7
Fig. S1 Relation between the amount of RuO ₂ loaded on TiO ₂ NWA and the content of RuCl ₃ in the reaction solution.	S8
Fig. S2 TEM image of the sample prepared by the impregnation method (<i>x</i> = 18).	S8
Fig. S3 HR-TEM image of the RuO ₂ film on TiO ₂ NW (<i>x</i> = 18).	S9
Fig. S4 Time course for OER on the ST-RuO ₂ (18)//TiO ₂ NWA electrode in 0.5 M H ₂ SO ₄ electrolyte solution.	S9
Fig. S5 OER polarization curves of Im-RuO ₂ //TiO ₂ NWA and TiO ₂ NWA for comparison in 0.5 M H ₂ SO ₄ electrolyte solution.	S10
Fig. S6 The equivalent circuit for the analysis of the Nyquist plots for the ST-RuO ₂ (<i>x</i>)//TiO ₂ NWA electrodes.	S10
Fig. S7 CV curves of the ST-RuO ₂ (3, 18)//TiO ₂ NWA electrodes, and the TiO ₂ NWA electrode for comparison in 0.1 M NaClO ₄ electrolyte solution degassed by argon bubbling.	S11
Fig. S8 Schematic representation of EC OER on the ST-RuO ₂ (3, 18)//TiO ₂ NWA electrodes.	S11
Fig. S9 Cyclic voltammograms of the Im-RuO ₂ (18)//TiO ₂ NWA (red) and ST-RuO ₂ (18)//TiO ₂ NWA (blue) electrodes.	S12
Fig. S10 Ru3d XP spectra for the ST-RuO ₂ (18)//TiO ₂ NWA electrode before and after 100 cycle electrolysis.	S12
Fig. S11 HR-TEM and HAADF-STEM images of the ST-RuO ₂ (18)//TiO ₂ NWA (blue) electrode after 100 cycle-electrolysis.	S13

Materials and experimental methods

Materials. Fluorine-doped tin(IV) oxide film-coated glass (FTO, TEC7), and Nafion film (Nafion 117, thickness = 0.007 inch) were purchased from Aldrich. Titanium tetra-n-butoxide ($\text{Ti}(\text{OBU})_4$, > 97.0%), hydrochloric acid (HCl , 35.0-37.0%), methyl alcohol (CH_3OH , > 99.8%), ethyl alcohol ($\text{C}_2\text{H}_5\text{OH}$, > 99.5%), sulfuric acid (H_2SO_4 , > 96.0%), potassium ferricyanide ($\text{K}_3[\text{Fe}(\text{CN})_6]$, > 99.0%), potassium hexacyanideferrate(II) trihydrate ($\text{K}_4[\text{Fe}(\text{CN})_6] \cdot 3\text{H}_2\text{O}$, > 99.5%), and ruthenium(IV) oxide (RuO_2 , >99.9) were purchased from Kanto Chemical Co. Ruthenium(III) chloride hydrate ($\text{RuCl}_3 \cdot x\text{H}_2\text{O}$ > 40% as Ru) was purchased from Tokyo Chemical Industry Co. All chemicals were used as received without further purification.

Electrode preparation. Rutile TiO_2 NWA was synthesized according to a previously reported method.^{S1} $\text{Ti}(\text{OBU})_4$ (0.17 mL) was dissolved in a 6 M HCl (10 mL), and stirred at room temperature (25°C) for 0.5 h. The solution was put into a Teflon-reactor (volume 25 mL), and FTO (3 pieces) was immersed into the solution. The Teflon-reactor was sealed in a stainless-autoclave, and heated at 423 K for 8 h. The resulting sample was washed with distilled water and acetone, and dried in vacuo at room temperature.

The $\text{RuO}_2//\text{TiO}_2$ NWA electrodes were prepared by a solvothermal-post heating method. RuCl_3 (1 ~ 50 mg) was added to a mixed solution of methanol (20 mL) and water (10 mL) in a Teflon-reactor (inner volume = 50 mL), and stirred at room temperature for 0.5 h. TiO_2 NWA-grown FTO plates (2 pieces) were immersed in the solution, and the Teflon-reactor was sealed in a stainless-autoclave. The autoclave was heated at 453 K for 6 h, and the resulting sample was washed with distilled water and acetone. After drying, the sample was calcined at 673 K for 10 h in the air.

For comparison, RuO_2 NP-loaded TiO_2 NWA ($\text{RuO}_2/\text{TiO}_2$ NWA) electrodes were prepared by the conventional impregnation method.^{S2} Commercial RuO_2 was dispersed into ethanol by ultrasonic irradiation for 0.5 h. After the suspension was dropped on TiO_2 NWA and dried at 323 K, the sample was calcined at 673 K for 10 h in the air.

Electrode characterization. To quantify the amount of Ru loading, $\text{RuO}_2//\text{TiO}_2$ NWA or $\text{RuO}_2/\text{TiO}_2$ NWA was immersed into 6 M HCl (10 mL) in a Teflon-reactor (volume 25 mL). The Teflon-reactor was sealed in a stainless-autoclave, and heated at 473 K for 12 h. The amount of Ru dissolved into the solution was quantified by inductively coupled plasma spectroscopy. Scanning electron microscopy (SEM) observation was carried out by using Hitachi SU8230 at an applied voltage of 20 kV. For transmission electron microscopy (TEM) observation, part of $\text{RuO}_2//\text{TiO}_2$ NWA or $\text{RuO}_2/\text{TiO}_2$ NWA was mechanically scraping off from the FTO substrate. TEM and high resolution-TEM images, HAADF-STEM images, EDS mapping were obtained by means of a JEOL JEM-2100F instrument at an applied voltage of 200 kV. X-ray photoelectron (XP) spectra were measured by means of a PHI VersaProbe 4 (ULVAC-PHI) with 15 kV and 3 mA using $\text{Al K}\alpha$ as X-ray source. The peak of $\text{C}1s$ (284.6 eV) was used for the energy correction. Diffuse reflectance UV-Vis-NIR spectra were measured using BaSO_4 as a reference (R_∞) by a UV-2600 spectrometer (Shimadzu) with an integrating sphere unit (Shimadzu, ISR-2600Plus). The spectra were transformed to the absorption spectra by the Kubelka-Munk function [$F(R_\infty) = (1 - R_\infty)^2/2R_\infty$]. X-ray diffraction (XRD) patterns were obtained at 40 kV and 100 mA using a Rigaku SmartLab X-ray diffractometer.

Electrocatalytic activity for OER. Electrochemical (EC) measurements were carried out by the two-component and three-electrochemical cell with the structure of $\text{RuO}_2//\text{TiO}_2$ NWA or $\text{RuO}_2/\text{TiO}_2$ NWA (working electrode), Ag/AgCl (reference electrode) | 0.5 M H_2SO_4 aqueous solution | Nafion | Pt film (counter electrode) in the dark. The active

area of working electrode is 1 cm^2 ($1 \text{ cm} \times 1 \text{ cm}$). The electrolyte solution was deaerated by argon gas bubbling for 30 min. The linear sweep voltammetry measurements were performed by means of a galvanostat/potentiostat (HZ-7000, Hokuto Denko) with scan rate = 20 mV s^{-1} . The amount of O_2 evolved was measured by gas chromatography (GC-2010Plus with BID-detector, Shimadzu) using a Rt-Mseive 5A column (Shimadzu GLC) with helium gas flow rate = 10 mL min^{-1} . Electrochemical impedance spectroscopy (EIS) measurements were carried out in the same EC cell using a frequency response analyzer (HZA-FRA1, Hokuto Denko) built in the galvanostat/potentiostat. The measurements were carried out with applying a 10 mV AC sinusoidal signal over the frequency range between 100 mHz and 100 kHz . The series resistance (R) and charge transfer resistance (R_{ct}) were estimated by a curve fitting for the Nyquist plots. The overpotential (η) was calculated from Eq. 1 by taking the IR drop.

$$\eta = E - I \times R \quad (1)$$

where R is the ohmic resistance determined by the EIS analysis.

Cyclic voltammograms. A three-electrode EC cell was fabricated with the structure of $\text{RuO}_2//\text{TiO}_2$ NWA (working electrode), Ag/AgCl (reference electrode) | 0.1 M NaClO_4 electrolyte solution containing $10 \text{ mM K}_3[\text{Fe}(\text{CN})_6]$ and $1 \text{ mM K}_4[\text{Fe}(\text{CN})_6]$ | Pt film (counter electrode). The active area of working electrode is 1 cm^2 ($1 \text{ cm} \times 1 \text{ cm}$). The electrolyte solution was deaerated by argon gas bubbling for 30 min. Cyclic voltammograms (CVs) were obtained by means of a galvanostat/potentiostat (HZ-7000, Hokuto Denko) with scan rate = 20 mV s^{-1} .

References

- S1. B. Liu and E. S. Aydil, Growth of oriented single-crystalline rutile TiO_2 nanorods on transparent conducting substrates for dye-sensitized solar cells. *J. Am. Chem. Soc.*, 2009, **131**, 3985-3990.
- S2. L. Manjakkal, K. Cvejin, J. Kulawik, K. Zaraska, D. Szwagierczak and G. Stojanovic, Sensing mechanism of $\text{RuO}_2\text{-SnO}_2$ Thick film pH sensors studied by potentiometric method and electrochemical impedance spectroscopy. *J. Electroanal. Chem.*, 2015, **759**, 82-90.

Table S1. Comparison of the mass-specific activity of ST-RuO₂//TiO₂ NWA and the RuO₂ electrodes. The electrolyte solution is 0.5 M H₂SO₄ aq.

Catalyst	Structure, morphology, and dimension of catalyst	Electrode (or support) and catalyst-electrode (or support) bonding mode	Preparation method	Loading amount ($\mu\text{g cm}^{-2}$)	Mass-specific Activity ($\text{A g}_{\text{cat}}^{-1}$) ^a	Ref.
RuO ₂	Single-crystal film / ~2.5 nm	Same as left (rutile-TiO ₂ nanowire array) / Chemical bond (heteroepitaxial junction)	Solvothermal	18	341	This work
RuO ₂ (photo)	Single-crystal film / ~2.5 nm	Same as left (rutile-TiO ₂ nanowire array) / Chemical bond (heteroepitaxial junction)	Solvothermal	21	718	This work
RuO ₂	Nanowire diameter 10~40 nm, length 100~200 nm	Glassy carbon (Graphitic carbon nitride) / Physical bond	Hydrothermal H ₂ O cast	171	92	S3
RuO ₂	---	Glassy carbon / Physical bond	H ₂ O cast	171	6.5	S3
RuO ₂	Particle / ~100 nm	Au film / Physical bond	Nafion cast	380	15	S4
RuO ₂	Particle / ~50 nm	Glassy carbon / Physical bond	Nafion cast	275	102	S5
RuO ₂	Particle / 5-8 nm	Glassy carbon / Physical bond	Nafion cast	404	19	S6
RuO ₂	Particle / 5-8 nm	Glassy carbon+carbon black / Physical bond	Nafion cast	317	89	S7
RuO ₂	Particle / 2 nm	Glassy carbon (Tungsten carbide) / Physical bond	Heat treatment Nafion cast	30	42	S8
RuO ₂	Particle / 2 nm	Glassy carbon / Physical bond	Nafion cast	510	6.7	S8
RuO ₂	Particle / 3 nm	Glassy carbon / Physical bond	Nafion cast	280	16	S9
RuO ₂	Particle / ~100 nm	Glassy carbon / Physical bond	Nafion cast	637	40	S10
RuO ₂	Nanorod / ~50 nm	Glassy carbon (anatase-TiO ₂ nanowire array) / Physical bond	Hydrothermal Nafion cast	126	171	S11
RuO ₂	Particle / ~50 nm	Glassy carbon / Physical bond	Nafion cast	195	34	S11
RuO ₂	Particle / ~8 nm	Glassy carbon (Carbonized polymer dot) / Physical bond	Heat treatment Nafion cast	510	58	S12
RuO ₂	Particle / ~2 nm	Glassy carbon (Graphene oxide) / Physical bond	Heat treatment Nafion cast	450	153	S13
RuO ₂	Particle / ~5 nm	Anatase-TiO ₂ nanowire array (Ti plate) / N/A	Hydrothermal Electrodeposition-calcination	246	21	S14

^a at 1.5 V vs RHE.

References

- S3. T. Bhowmik, M. K. Kundu and S. Barman, Growth of one-dimensional RuO₂ nanowires on g-carbon nitride: an active and stable bifunctional electrocatalyst for hydrogen and oxygen evolution reactions at all pH values. *ACS Appl. Mater. Interfaces*, 2016, **8**, 28678-28688.
- S4. T. Audichon, T. W. Nappom, C. Canaff, C. Morais and C. Comminges, IrO₂ coated on RuO₂ as efficient and stable electroactive nanocatalysts for electrochemical water splitting. *J. Phys. Chem. C*, 2016, **120**, 2562-2573.
- S5. S. Chen, H. Huang, P. Jiang, K. Yang, J. Diao, S. Gong, S. Liu, M. Huang, H. Wang and Q. Chen, Mn-doped RuO₂ nanocrystals as highly active electrocatalysts for enhanced oxygen evolution in acidic media. *ACS Catal.*, 2020, **10**, 1152-1160.
- S6. L. Zhang, H. Jang, H. Liu, M. G. Kim, D. Yang, S. Liu, X. Liu and J. Cho, Sodium-decorated amorphous/crystalline RuO₂ with rich oxygen vacancies: a robust pH-universal oxygen evolution electrocatalyst. *Angew. Chem. Int. Ed.*, 2021, **60**, 18821-18829.
- S7. Y. Wen, C. Liu, R. Huang, H. Zhang, X. Li, F. García de Arquer, Z. Liu, Y. Li and B. Zhang, Introducing Brønsted acid sites to accelerate the bridging-oxygen-assisted deprotonation in acidic water oxidation. *Nat. Commun.*, 2022, **13**, 4871.
- S8. S.-C. Sun, H. Jiang, Z.-Y. Chen, Q. Chen, M.-Y. Ma, L. Zhen, B. Song and C.-Y. Xu, Bifunctional WC-supported RuO₂ nanoparticles for robust water splitting in acidic media. *Angew. Chem. Int. Ed.*, 2022, **61**, e202202519.
- S9. Wang, K.; Wang, Y.; Yang, B.; Li, Z.; Qin, X.; Zhang, Q.; Lei, M.; Wu, G.; Hou, Y. Highly Active Ruthenium Sites Stabilized by Modulating Electron-Feeding for Sustainable Acidic Oxygen-Evolution Electrocatalysis. *Energy. Environ. Sci.* **2022**, *15*, 2356-2365.
- S10. K. Wang, Y. Wang, B. Yang, Z. Li, X. Qin, Q. Zhang, M. Lei, G. Wu and Y. Hou, Highly active ruthenium sites stabilized by modulating electron-feeding for sustainable acidic oxygen-evolution electrocatalysis. *Energy. Environ. Sci.*, 2022, **15**, 2356-2365.
- S11. J. Zhang, R. Lin, Y. Zhao, H. Wang, S. Liu and X. Cai, Modulation for RuO₂/TiO₂ via simple synthesis to enhance the acidic oxygen evolution reaction. *ACS Sustainable Chem. Eng.*, 2023, **11**, 9489-9497.
- S12. T. Feng, J. Yu, D. Yue, H. Song, S. Tao, G. I. N. Waterhouse, S. Lu and B. Yang, Defect-rich ruthenium dioxide electrocatalyst enabled by electronic reservoir effect of carbonized polymer dot for remarkable pH-universal oxygen evolution. *Appl. Catal. B*, 2023, **328**, 122546.
- S13. Y. Wang, R. Yang, Y. Ding, B. Zhang, H. Li, B. Bai, M. Li, Y. Cui, J. Xiao and Z.-S. Wu, Unraveling oxygen vacancy site mechanism of Rh-doped RuO₂ catalyst for long-lasting acidic water oxidation. *Nat. Commun.*, 2023, **14**, 1412.
- S14. Y. Liu, T. Duan, L. Xu, X. Gao, L. Xue, Y. Xin, L. Ma, G. Huang and T. Liu, Electrocatalyst of RuO₂ decorating TiO₂ nanowire arrays for acidic oxygen evolution. *Int. J. Hydrogen Energy.*, 2023, **48**, 10737-10754.

Table S2. Peak area ratio of O1s-XP signals for ST-RuO₂(*x*)/TiO₂ NWA and Im-RuO₂/TiO₂ electrodes.

Electrode	O (TiO ₂)	O (RuO ₂)	Surface OH	$I_{\text{RuO}_2}/I_{\text{TiO}_2}$ ^a
TiO ₂ NWA	67.3	---	32.7	---
ST-RuO ₂ (3)/TiO ₂ NWA	83.1	2.5	14.4	0.03
ST-RuO ₂ (10)/TiO ₂ NWA	38.5	37.2	24.3	0.97
ST-RuO ₂ (18)/TiO ₂ NWA	18.8	41.6	39.6	2.21
ST-RuO ₂ (25)/TiO ₂ NWA	30.7	39.0	30.3	1.27
ST-RuO ₂ (43)/TiO ₂ NWA	32.8	34.5	32.7	1.05
Im-RuO ₂ (18)/TiO ₂ NWA	77.8	5.1	17.1	0.07
RuO ₂ particles	---	56.6	43.4	---

^a I_{RuO_2} and I_{TiO_2} are the O1s peak areas of RuO₂ and TiO₂, respectively.

Table S3. EIS parameters for ST-RuO₂(*x*)/TiO₂ NWA and Im-RuO₂/TiO₂ electrodes.

Electrode	R (Ω)	CPE index (α)	CPE constant (F s ^(α-1))	R_{ct} (Ω)
TiO ₂ NWA	11.9	0.80	9.2×10^{-6}	1.2×10^4
ST-RuO ₂ (3)/TiO ₂ NWA	25.7	0.92	9.0×10^{-6}	250
ST-RuO ₂ (10)/TiO ₂ NWA	13.6	0.61	4.9×10^{-5}	38
ST-RuO ₂ (18)/TiO ₂ NWA	15.3	0.82	1.4×10^{-3}	4.9
ST-RuO ₂ (25)/TiO ₂ NWA	30.3	0.83	1.0×10^{-3}	9.7
ST-RuO ₂ (43)/TiO ₂ NWA	20.0	0.67	2.0×10^{-3}	39
Im-RuO ₂ (18)/TiO ₂ NWA	13.9	0.85	6.9×10^{-6}	920

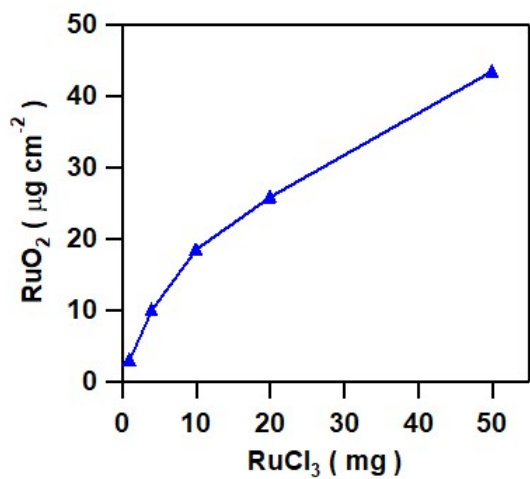


Fig. S1 Relation between the amount of RuO₂ loaded on TiO₂ NWA and the content of RuCl₃ in the reaction solution. The ST-reaction time was fixed at 8 h.

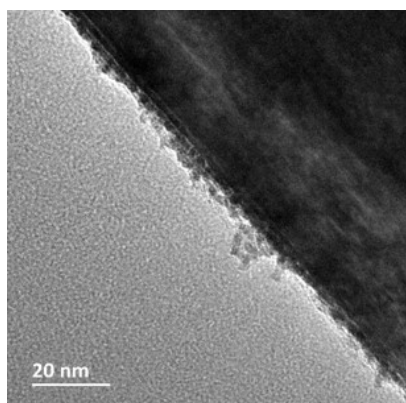


Fig. S2 TEM image of the sample prepared by the impregnation method ($x = 18$).

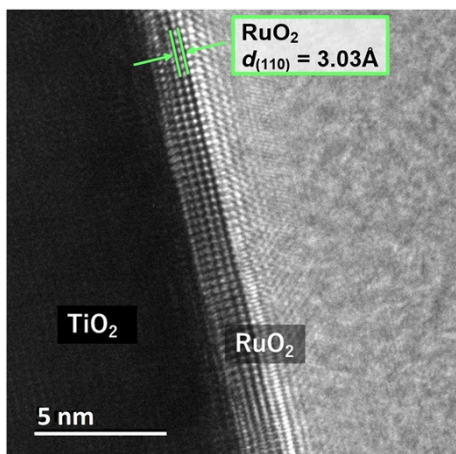


Fig. S3 HR-TEM image of the RuO₂ film on TiO₂ NW ($x = 18$).

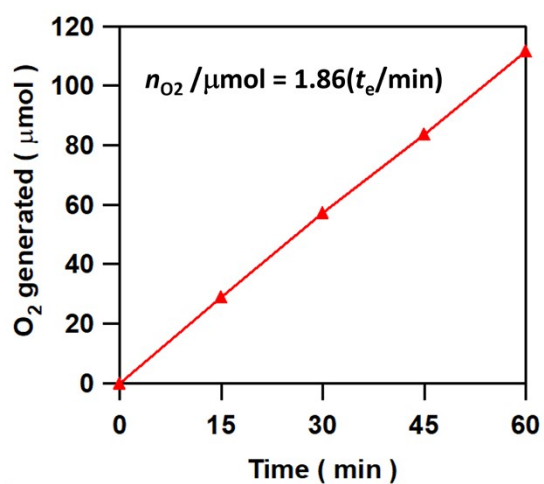


Fig. S4 Time course for OER on the ST-RuO₂(18)//TiO₂ NWA electrode in 0.5 M H₂SO₄ electrolyte solution. The straight line shows the amount of O₂ generated with 100% Faradaic efficiency.

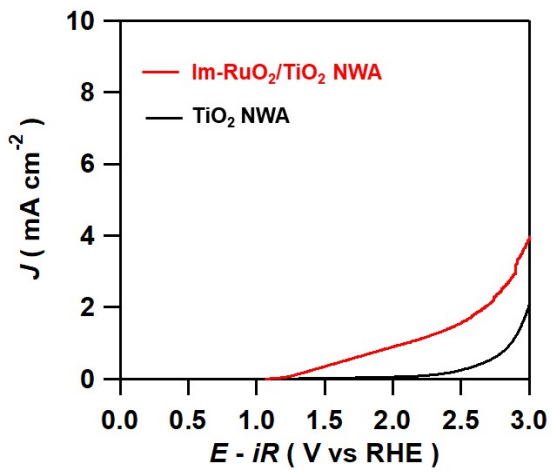


Fig. S5 OER polarization curves of $\text{Im-RuO}_2/\text{TiO}_2$ NWA and TiO_2 NWA for comparison in 0.5 M H_2SO_4 electrolyte solution.

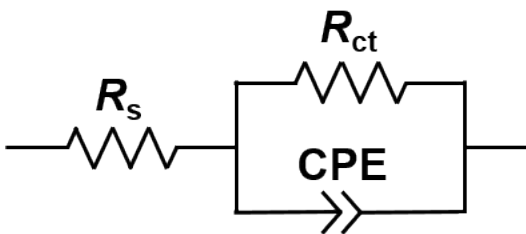


Fig. S6 The equivalent circuit for the analysis of the Nyquist plots for the $\text{ST-RuO}_2(x)/\text{TiO}_2$ NWA electrodes.

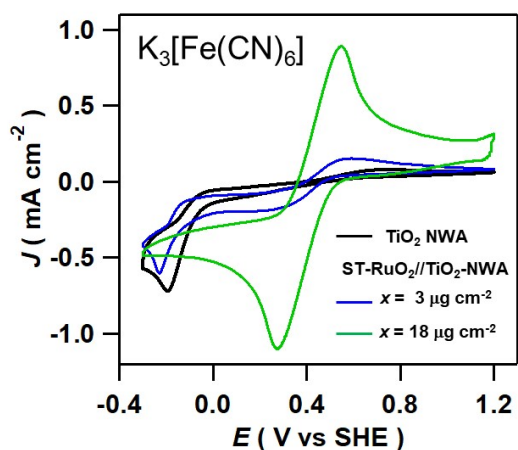


Fig. S7 CV curves of the ST-RuO₂(3, 18)//TiO₂ NWA electrodes, and the TiO₂ NWA electrode for comparison in 0.1 M NaClO₄ electrolyte solution degassed by argon bubbling.

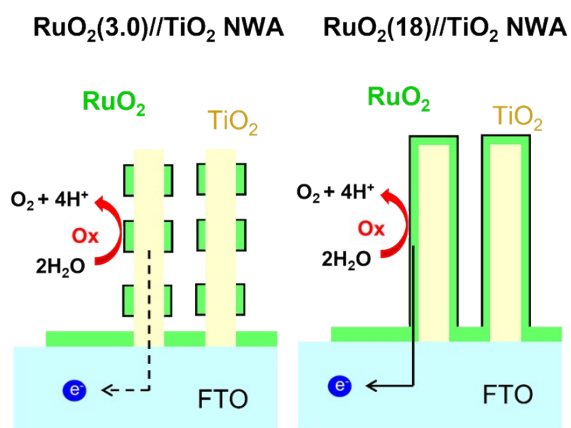


Fig. S8 Schematic representation of EC OER on the ST-RuO₂(3, 18)//TiO₂ NWA electrodes.

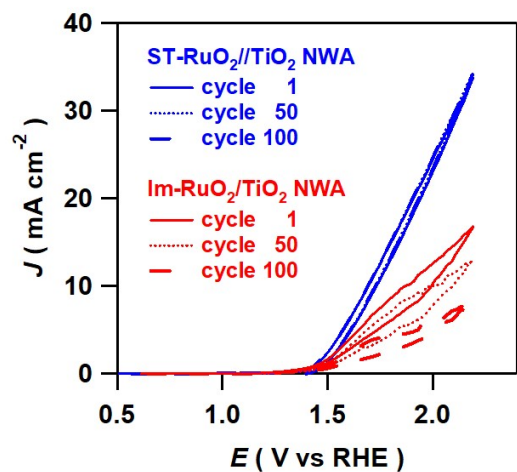


Fig. S9 Cyclic voltammograms of the Im-RuO₂(18)/TiO₂ NWA (red) and ST-RuO₂(18)/TiO₂ NWA (blue) electrodes.

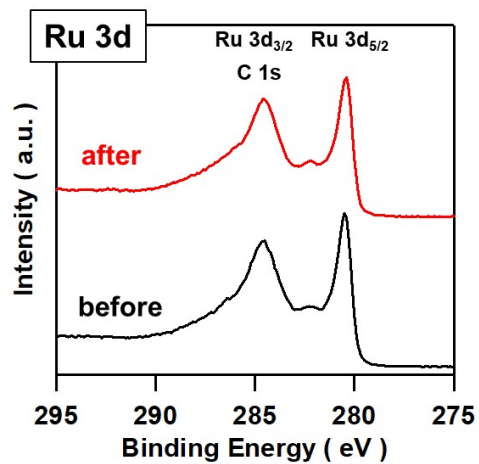


Fig. S10 Ru3d XP spectra for the ST-RuO₂(18)/TiO₂ NWA electrode before and after 100 cycle electrolysis.

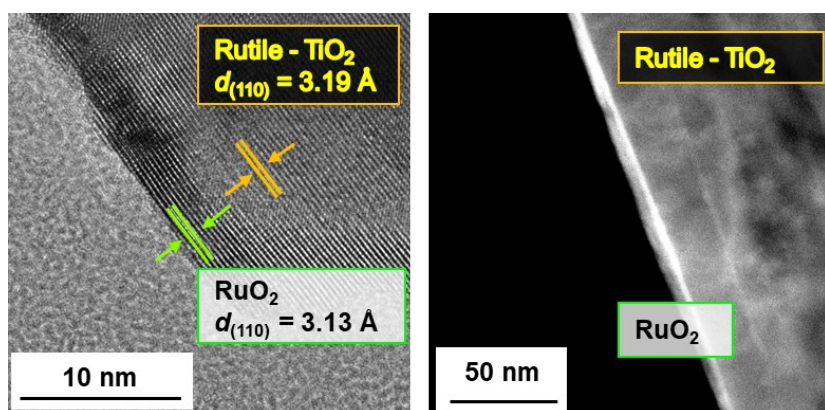


Fig. S11 HR-TEM and HAADF-STEM images of the ST-RuO₂(18)//TiO₂ NWA (blue) electrode after 100 cycle-electrolysis.